Scripta Materialia 166 (2019) 19–23

Contents lists available at ScienceDirect

Scripta Materialia

journal homepage: www.elsevier.com/locate/scriptamat

Exploring the thermal stability of a bimodal nanoscale multilayered system

J. Sebastian Riano [a], Andrea M. Hodge [a,b,*]

[a] Department of Chemical Engineering and Materials Science, University of Southern California, 3650 McClintock Ave., Los Angeles, CA 90089, USA
[b] Department of Aerospace and Mechanical Engineering, University of Southern California, Los Angeles, CA 90089, USA

ARTICLE INFO

Article history:
Received 18 December 2018
Received in revised form 3 February 2019
Accepted 25 February 2019
Available online xxxx

Keywords:
Bimodal nanometallic multilayers
Thermal stability
Interfaces
Brick-like grains
Nanomaterials

ABSTRACT

The thermal stability of bimodal Ta-Hf nanometallic multilayers, comprised of columnar and brick-like grains, was explored by characterizing films annealed at 550 °C and 1000 °C. Although the brick-like grains recrystallized, their grain size remained in the nanoscale. Recrystallization of the columnar grains was hindered by semi-coherent sub-grain boundaries and quadrupole points. Growth of the recrystallized brick-like grains was prevented by Hf precipitates, which activated kinetic and thermodynamic stabilization mechanisms. The present results outline a promising route to improve the stability of nanomaterials by using bimodal nanometallic multilayers with engineered interfaces while expanding the available architectures to synthesize nanocrystalline materials.

Nanocrystalline materials have exceptional mechanical, optical, electrical, and catalytic properties that have potential for new applications such as sensor devices, capacitors, catalyzers, or protective coatings [1–3]. However, nanocrystalline materials have a high density of interfaces that at elevated temperatures induce microstructural transformations, which results in degradation of the interesting properties inherent to nanomaterials [4]. Thus, several studies have attempted to improve the thermal properties of nanomaterials via kinetic and thermodynamic approaches [5,6]. First, in a kinetic route the stability is increased by inducing the formation of precipitates that pin the grain boundaries and thus reduce their migration velocity. Second, in thermodynamic stabilization the grain boundary energy, which is the driving force for grain boundary motion, is decreased via solute segregation to the grain boundaries [7]. Another alternative is to use special architectures that decrease the interface energy like low angle grain boundary nanolaminates and nano multilayers [8]. In addition, a recent study by Zhou et al. suggests that the thermal stability of nanocrystalline materials could be improved by decreasing the grain size below a critical value, under which the interface energy is lowered due to the activation of dislocations via annealing [9].

In regards to special architectures or engineered structures, nanometallic multilayers (NMMs) are a potential route towards enhanced thermal stability, improved strength, and better radiation resistant materials [10–14]. NMMs are aggregates of alternating nanometric metallic layers of different composition that can be used to control variables that influence the thermal evolution of nanomaterials such as the density of interphases, the local composition, and the grain structure, which can be columnar, equiaxed or compressed. Where compressed grains are cylindrical grains that resemble a brick wall in two-dimensional micrographs, henceforth these grains will be referred to as brick-like grains [15,16]. Previous research suggests that NMMs with columnar grains show increased thermal stability. For example, studies on columnar grained Hf-Ti, W-Cr, Mo-Au, and Cu-Co NMMs, have demonstrated that during annealing, thermodynamic or kinetic stabilization mechanisms can be activated, leading to the retention of nanoscale features [13,17–20]. Research on brick-like grained NMMs systems, such as Cu-Ta, Cu-Nb, Al-Ni, and Cu-Ag, have shown that this type of structure can increase the recrystallization temperature [21–27]. Overall, most studies have pointed out that NMMs with thicker layers and columnar grains have greater stability [23,24,28].

Although NMMs with either columnar or brick-like grains have been studied individually, to the best of the authors' knowledge, there is no previous research on NMMs with a bimodal grain structure. Previous studies of bimodal materials have focus on microstructures with two grain size distributions which combined the high strength of nanocrystalline materials and the increased ductility of ultrafine grain materials [29–31]. These microstructures have been used to enhance the mechanical properties of nanocrystalline pure Cu, Ti, Zr, and Ni, as well as Cu-Al, Cu-Ag, Al-Mg, and Ti-Zr alloys [32–41]. Despite the fact that there is limited research on the thermal stability of bimodal materials, a study on the magnesium alloy AZ91 shows that the combination of two grain sizes promotes the development of low angle grain boundaries, which

* Corresponding author at: Department of Chemical Engineering and Materials Science, University of Southern California, 3650 McClintock Ave., Los Angeles, CA 90089, USA.
E-mail address: ahodge@usc.edu (A.M. Hodge).

https://doi.org/10.1016/j.scriptamat.2019.02.043
1359-6462/

exhibit higher thermal stability [42,43]. Thus, a system with both NMMs and a bimodal grain structure could provide increased microstructural stability.

Therefore, the aim of this study is to explore the thermal stability of Ta-Hf bimodal NMMs by performing a detailed microstructural investigation at different annealing temperatures. In this manuscript, bimodal NMMs are defined as nanolayered composites comprised of two different regions with columnar and brick-like grains that can be synthesized by interrupting the growth of columnar grains during deposition. The Ta-Hf system was selected due to its proclivity for nanocrystalline stability and also because it favors the formation of columnar grains, which facilitates the deposition of a bimodal structure [44].

Ta-Hf bimodal multilayers (2.0 μm thick) were deposited on Si (100) substrates by direct current (DC) magnetron sputtering inside a vacuum chamber evacuated to a base pressure of 1.1×10^{-4} Pa. During deposition, the chamber was filled with 6.7×10^{-1} Pa of Ar to sputter the individual layers using powers of 175.0 W and 50.0 W for Ta (99.95 at. % Ta) and Hf (99.9 at. % Hf) sources, respectively. Under these conditions, the deposition rates were approximately 30 nm/min for Ta and 9 nm/min for Hf, values which were held constant during the sputtering procedure. The composition of the alternating 2 nm Hf (99.9 at. % Hf) and 14 nm Ta-Hf (14.6 at. % Hf) layers was adjusted by controlling the sputtering time of the Ta source as indicated in a previous manuscript [17]. The global composition of the film (22.4 at. % Hf) was measured using an energy dispersive x-ray (EDS) EDAX detector inside a JSM-7001 scanning electron microscope (SEM). X-ray diffractometry measurements using a Rigaku Ultima IV diffractometer revealed a highly BCC (110) texture. To study the morphology of the films, TEM lamellas were prepared by focus ion beam (FIB) using a FIB-4500 (JEOL). Subsequently, these TEM samples were characterized using a JEM-2100F (JEOL) microscope.

The microstructure of the Ta-Hf bimodal NMMs, presented in Fig. 1a, is comprised of columnar grains at the top of the film (Fig. 1b) and brick-like grains (Fig. 1c) that extend over 600 nm from the substrate surface; this structure corresponds to a film type Zone 1 in the Thornton diagram [45]. The selected area diffraction (SAD) pattern from the cross-section of the film (top of Fig. 1a) only showed Ta rings diffracted from the solid solution in the Ta rich layers. This indicates either that the pure Hf layers are not large enough to diffract sufficient electrons to observe a ring, or that most of the pure Hf layers are adopting the BCC structure that has been observed in other studies [46,47]. The morphology of the columnar and brick-like grains was identified by dark field TEM images (Fig. 1d–e) that were also used to measure grain size distributions for each type of grain (Fig. 1f–g) following procedures outlined in a previous manuscript [17]. From these distributions, an average grain size of 109 ± 43 nm and 31 ± 9 nm (Average grain size ± Standard Error) were calculated for columnar and brick-like grains, respectively [48].

The structure of the interphases within these types of grains depends on the surface energy (γ) and the atomic radius (a) of the individual metals A and B at the interface [49]. When the surface energy mismatch ($\Gamma_{AB} = 2(\gamma_A - \gamma_B)/(\gamma_A + \gamma_B)$) is $\Gamma_{AB} < 0.5$ and the ratio of atomic radii ($r = a_A/a_B$) is $r \lesssim 1.00$, relatively stable coherent (5–200 mJ m^{-2}) or semi-coherent (200–800 mJ m^{-2}) interphases form between the subgrains of uninterrupted columnar structures [49,50]. For example, in studies performed on Hf-Ti ($\Gamma_{Hf,\ Ti} = -0.06$, $r_{Hf,\ Ti} = 1.08$) and W-Cr ($\Gamma_{W,\ Cr} = 0.13$ $r_{W,\ Cr} = 0.96$) NMMs, the columnar grains are comprised of subgrains bounded by semi-coherent interfaces [17,18]. In contrast, when $\Gamma_{AB} > 0.5$, highly mobile incoherent interphases (800–2500 mJ m^{-2}) can interrupt columnar grain structure or drive the formation of azimuthally misoriented brick-like grains [51–53]. For instance, it was observed that in a Mo-Au NMMs study ($\Gamma_{Mo,\ Au} = 0.92$, $r_{Mo,\ Au} = 1.07$), the columnar grains are interrupted by incoherent interphases between the Mo rich and pure Au layers [20]. Therefore, different elements promote the formation of certain interphases that can be used to tailor NMMs with specific grain structures.

Particularly, in the high resolution TEM (HRTEM) images of the Ta-Hf NMMs in Fig. 2, it is observed that the interphases between layers in the columnar and brick-like regions have different atomic structures. For this system ($\Gamma_{Ta,\ Hf} = 0.22$, $r_{Ta,\ Hf} = 0.96$), the aforementioned variables imply that this system favors the formation of semi-coherent interphases within uninterrupted columnar grains [52,53]. However, under the sputtering conditions used (Zone 1 of the Thornton diagram), shadowing due to substrate roughness and limited surface diffusion prevent the development of columnar grains at the bottom of the film [54]. Therefore, close to the substrate the deposition of Hf layers effectively interrupts the growth of coalesced Ta rich islands that become

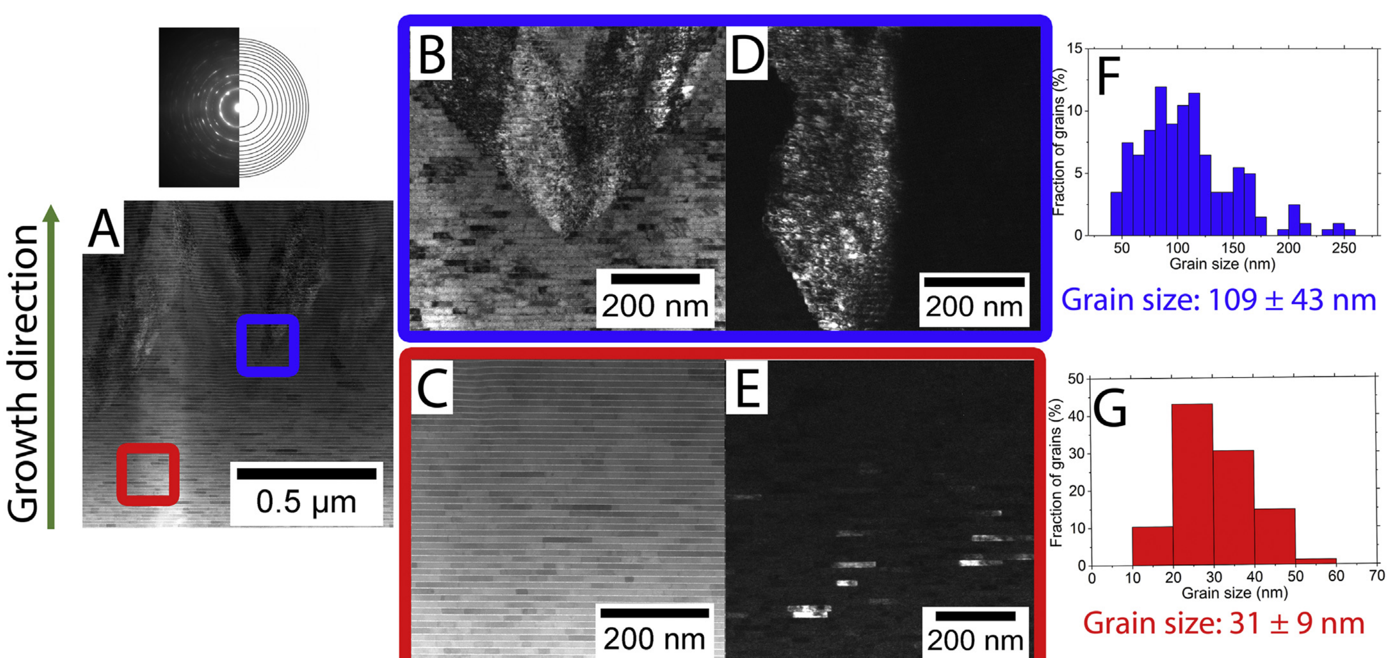

Fig. 1. Bright field TEM images showing (a) the bimodal multilayers, (b) columnar grains at the top, and (c) brick-like grain at the bottom of the film. The dark-field TEM images display the corresponding grain morphologies for (d) columnar and (e) brick-like regions. The grain size distributions for the columnar and the brick-like grains are shown in (f) and (g) respectively.

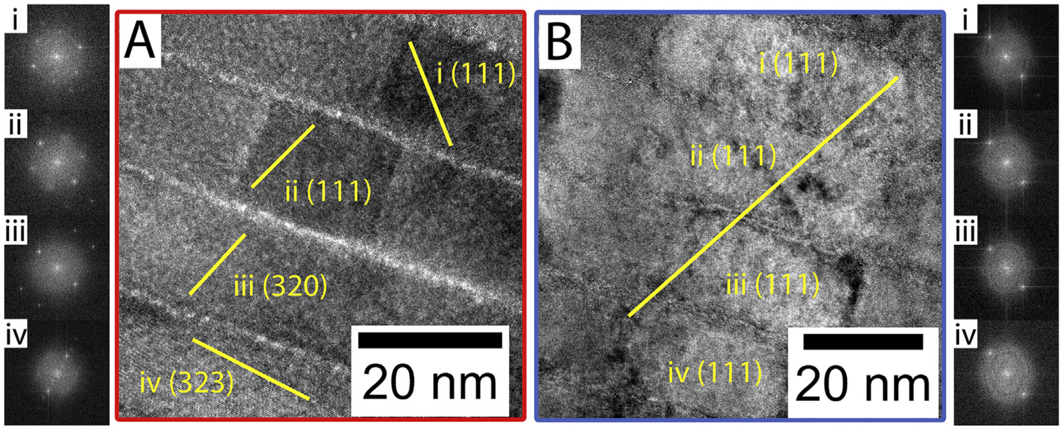

Fig. 2. High resolution TEM images of (a) the brick-like grains, showing atomic lattices that extend over a single layer, and of (b) the columnar grains, displaying atomic layers extending over several layers. The yellow lines indicate the orientation of atomic layers inside the grains. The FFT patterns (i) to (iv) show that the brick like grains in consecutive layers have different orientations, while the patterns from (v) to (viii) indicate that the columnar subgrains have the same orientation. (For interpretation of the references to colour in this figure legend, the reader is referred to the web version of this article.)

brick-like grains. Specifically, Fig. 2a shows that these grains have different orientations in consecutive layers (see Fast Fourier Transform or FFT patterns) and are surrounded by high-angle grain boundaries, which have higher contrast and definition in HRTEM images [55,56]. As the film continues to grow, shadowing effects reduce the uniformity of the Hf layers, and in turn these layers less effectively interrupt the growth of Ta-rich islands, which continue to grow in the form of columnar grains that extend over several layers. For instance, Fig. 2b, highlights a columnar grain at the top of the film comprised of Ta rich subgrains in the (111) zone axis (see FFT patterns) with diffuse semi-coherent pure Hf layers between the subgrains [54]. Furthermore, the heterogenous distribution of brick-like and columnar grains makes the density of high-angle grain boundaries greater at the bottom of the film, which results in a non-uniform distribution of stresses [57]. Accordingly, profilometry measurements show that the as-sputtered films are in a compressed state with average residual stresses of −745.6 MPa (Stoney's equation) [58].

In order to study the evolution of the bimodal microstructures under thermal loading, the as-sputtered samples were heat-treated under vacuum at 550 °C and 1000 °C, keeping the temperature constant for 96 h and quenching the films in a low vapor pressure oil without breaking vacuum (Invoil 705, Inland Vacuum Industries). These temperatures were selected from DSC scans of the system, where a thermal event occurring between 482 °C and 842 °C with $\Delta H = -9.6$ kJ/mol was identified. The scans were collected using a Labsys thermal analyzer, by heating the films at a constant rate of 10 °C/min from 20 °C to 1000 °C under constant Ar flow of 40 ml/min. The microstructure of the samples annealed at 550 °C and 1000 °C, are presented in the bright field TEM micrographs in Fig. 3a and e, which are comprised of columnar grains at the top of the film and equiaxed grains at the bottom. It can be

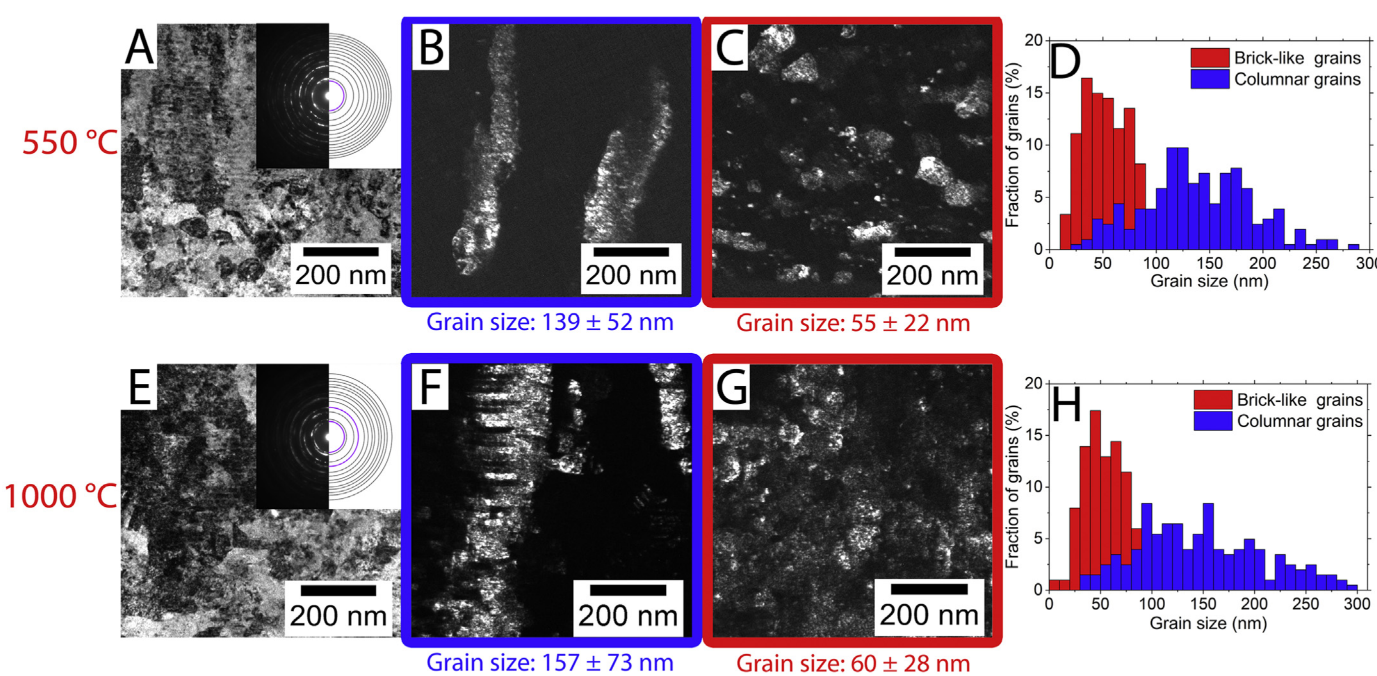

Fig. 3. Bight field, dark field TEM and corresponding grain size distributions of the multilayers annealed at 550 °C (a,b,c and d), and at 1000 °C (e,f,g and h) after 96 h. The insets in (a) and (e) show the corresponding SAD patterns with the Hf rings colored purple. The dark-field TEM images indicate that while at both temperature the structure of the columnar is preserved, most of the brick-like grains have recrystallized at 500 °C. Similar grain size distributions are observed at 550 °C (d) and at 1000 °C (g) suggesting no significant grain growth. (For interpretation of the references to colour in this figure legend, the reader is referred to the web version of this article.)

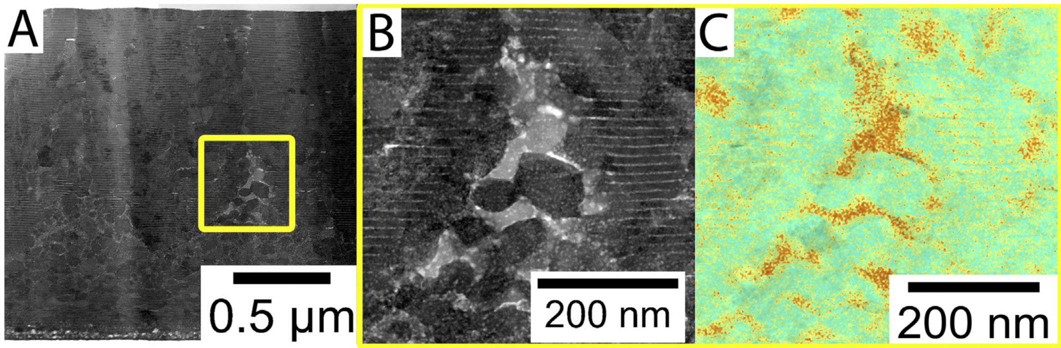

Fig. 4. (a) Bright field STEM image highlighting the structure of the multilayered samples after annealing at 1000 °C, where the yellow box indicates an area with both columnar and brick-like grains. This region was studied in more detail by collecting additional (b) STEM images and (c) EDS maps, which display Ta rich grains (Turquoise) surrounded by Hf precipitates (Orange). (For interpretation of the references to colour in this figure legend, the reader is referred to the web version of this article.)

observed that the columnar grains conserve their multilayered structure (Fig. 3b and f), although, the pure Hf layers show several breakthroughs, suggesting that roughening has occurred during annealing [59]. At 550 °C the equiaxed grains at the bottom of the film (Fig. 3c) do not show any multilayers, which indicates that the exothermic transformation identified in the DSC scans corresponds to recrystallization of the brick-like grains. This process is driven by the strain energy and the greater mobility of the incoherent high-angle grain boundaries [43,60,61]. Furthermore, the SAD patterns at 550 °C (Inset Fig. 3a) show a new Hf (100) ring, which points to the segregation and clustering of Hf at grain boundaries during recrystallization [62]. Subsequently, at 1000 °C, the equiaxed grains have spheroidized (Fig. 3g) and the Hf clusters have agglomerated to form precipitates at the grain boundaries, which diffract an additional Hf (102) ring (Inset Fig. 3e) [62]. Dark-field TEM images were used to calculate the grain size distributions between 500 °C and 1000 °C (Fig. 3d and h). The measurements show that the average size of the columnar grains moderately increases from 139 $\pm$ 52 nm to 157 $\pm$ 73 nm, and that of the equiaxed grains grow from 55 $\pm$ 32 nm to 60 $\pm$ 28 nm, respectively.

The aforementioned results seem to indicate that a bimodal NMM structure can enhance the thermal stability of the Ta-Hf system via mechanisms that depend on the interface structure. The boundaries of the columnar subgrains are locked by the semi-coherent pure Hf layers, which have lower mobility [63]. These layers intersect high-angle grain boundaries at quadrupole points, which prevent the formation of grooves and decrease the strain at the columnar grains, thus lowering the driving force for recrystallization [28]. This type of stabilization has been studied in detail by comparing the thermal evolution of Cu-Nb NMMs with either staggered or vertically aligned grains [23,28,64,65]. In addition, the equiaxed grains are stabilized by the Hf precipitates, which lock the grain boundaries and reduce their energy, resulting in the simultaneous activation of kinetic and thermodynamic stabilization mechanisms that have been reported for other systems such as Mo-Au, Cu-Ta, and Cu-Nb [20,66,67]. Specifically, at 1000 °C, the Hf precipitates inside the area highlighted in Fig. 4a were studied in more detail. Fig. 4b, a TEM micrograph of that area, shows a combination of columnar grains with well-defined layers and equiaxed grains, which are surrounded by precipitates that display compositional contrast. The corresponding EDS map (Fig. 4c), where Hf is colored orange and Ta turquoise, highlights that while the equiaxed grains are enriched with Ta, the precipitates along the grain boundaries are Hf rich. These precipitates form a wetting complexion that reduces the energy and the mobility of the grain interfaces and results in the combined stabilization of the equiaxed grain boundaries, in agreement with predictions from the Murdoch and Schuh model for the Ta-Hf system [44,68,69]. Furthermore, as the equiaxed grains spheroidize, their shape tends towards polyhedrons that minimize the grain boundary area and increase the stability of the system [63,70]. It should also be noted that an increased temperature threshold for grain coarsening has been reported for grain sizes below a critical value [9]. Although that particular study focused on pure Cu and Ni systems with critical grain sizes of 70 nm and 90 nm, respectively, the small grain size of the brick-like grains could also be increasing the temperature needed for grain growth.

In this manuscript we explore for the first time, the thermal stability of bimodal Ta-Hf NMMs with both columnar and equiaxed grains. It was observed that a bimodal microstructure enhances the thermal stability by providing several stabilizing mechanisms that depend on the interface structure. For example, the stability of the columnar grains is increased by quadrupole points that lock the grain boundaries and by the presence of semi-coherent Hf layers, which prevent recrystallization. Although the brick-like grains recrystallize between 482 °C and 842 °C, the new equiaxed grains are stabilized by Hf rich precipitates at the grain boundaries, which simultaneously activate kinetic and thermodynamic stabilization mechanisms. Overall, both columnar and brick-like grains show minimal grain growth, where even at 1000 °C the grain size of the columnar grain is 157 $\pm$ 73 nm and that of the brick-like grains is 60 $\pm$ 28 nm. These results highlight a path to improve the stability of nanocrystalline materials using bimodal NMMs with engineered interface structures.

This work was performed under the auspices of the National Science Foundation under Grant DMR-1709771 and of the Office of Naval Research under Grant N00014-12-1-0638. We acknowledge the Center for Electron Microscopy and Microanalysis at USC for the use of their SEM, FIB and TEM instruments.

References

[1] H. Gleiter, Prog. Mater. Sci. 33 (4) (1989) 223–315.
[2] E. Ringe, IUCrJ 1 (6) (2014) 530–539.
[3] C. Suryanarayana, Adv. Eng. Mater. 7 (11) (2005) 983–992.
[4] R.A. Andrievski, Russ. Chem. Rev. 83 (4) (2014) 365–375.
[5] H.R. Peng, M.M. Gong, Y.Z. Chen, F. Liu, Int. Mater. Rev. 62 (6) (2017) 303–333.
[6] C.C. Koch, R.O. Scattergood, M. Saber, H. Kotan, J. Mater. Res. 28 (13) (2013) 1785–1791.
[7] T. Chookajorn, H.A. Murdoch, C.A. Schuh, Science 337 (6097) (2012) 951–954.
[8] K. Lu, Nat. Rev. Mater. 1 (5) (2016).
[9] X. Zhou, X.Y. Li, K. Lu, Science 360 (6388) (2018) 526–530.
[10] W. Han, M.J. Demkowicz, N.A. Mara, E. Fu, S. Sinha, A.D. Rollett, Y. Wang, J.S. Carpenter, I.J. Beyerlein, A. Misra, Adv. Mater. 25 (48) (2013) 6975–6979.
[11] S. Subedi, I.J. Beyerlein, R. LeSar, A.D. Rollett, Scr. Mater. 145 (Supplement C) (2018) 132–136.
[12] I.J. Beyerlein, A. Caro, M.J. Demkowicz, N.A. Mara, A. Misra, B.P. Uberuaga, Mater. Today 16 (11) (2013) 443–449.
[13] M.N. Polyakov, T. Chookajorn, M. Mecklenburg, C.A. Schuh, A.M. Hodge, Acta Mater. 108 (2016) 8–16.
[14] C. Weisbuch, Physics, fabrication, and applications of multilayered structures, Springer Science & Business Media2013.
[15] B.M. Clemens, H. Kung, S.A. Barnett, MRS Bull. 24 (2) (1999) 20–26.
[16] C.M. Falco, Metallic multilayers and superlattices, Festkörperprobleme 25, Springer1985, pp. 531–537.
[17] J.S. Riano, A.M. Hodge, Scr. Mater. 142 (2018) 55–60.
[18] J.S. Riano, A.M. Hodge, Materialia 2 (2018) 190–195.
[19] M. Hecker, J. Thomas, D. Tietjen, S. Baunack, C.M. Schneider, Q. An, N. Cramer, R.E. Camley, Z. Celinski, J. Phys. D. Appl. Phys. 36 (5) (2003) 564.

[20] J.A. Bahena, J. Sebastian Riano, M.R. Chellali, T. Boll, A.M. Hodge, Materialia 4 (2018) 157–165.
[21] L.F. Zeng, R. Gao, Q.F. Fang, X.P. Wang, Z.M. Xie, S. Miao, T. Hao, T. Zhang, Acta Mater. 110 (2016) 341–351.
[22] J.S. Carpenter, S.J. Zheng, R.F. Zhang, S.C. Vogel, I.J. Beyerlein, N.A. Mara, Philos. Mag. 93 (7) (2013) 718–735.
[23] A. Misra, R.G. Hoagland, J. Mater. Res. 20 (08) (2005) 2046–2054.
[24] Y.J. Ma, M.Z. Wei, C. Sun, Z.H. Cao, X.K. Meng, Mater. Sci. Eng. A 686 (2017) 142–149.
[25] A. Misra, J.P. Hirth, R.G. Hoagland, Acta Mater. 53 (18) (2005) 4817–4824.
[26] A.C. Lewis, D. Josell, T.P. Weihs, Scr. Mater. 48 (8) (2003) 1079–1085.
[27] D.R. Economy, B.M. Schultz, M.S. Kennedy, J. Mater. Sci. 47 (19) (2012) 6986–6991.
[28] H.B. Wan, Y. Shen, J. Wang, Z.Q. Shen, X.J. Jin, Acta Mater. 60 (19) (2012) 6869–6881.
[29] H.-M.Z. Min Zha, Yu Zhi-Yuan, Xuan-He Zhang, Xiang-Tao Meng, Hui-Yuan Wang, Qi-Chuan Jiang, J. Mater. Sci. Technol. 34 (2) (2018) 257–264.
[30] C.C. Koch, Ductility in nanostructured and ultra fine-grained materials: recent evidence for optimism, J. Metastable Nanocryst. Mater., Trans Tech Publ, 2003, pp. 9–20.
[31] S. Shukla, D. Choudhuri, T. Wang, K. Liu, R. Wheeler, S. Williams, B. Gwalani, R.S. Mishra, Math. Res. Lett. 6 (12) (2018) 676–682.
[32] Y. Wang, M. Chen, F. Zhou, E. Ma, Nature 419 (2002) 912.
[33] K. Sitarama Raju, V. Subramanya Sarma, A. Kauffmann, Z. Hegedűs, J. Gubicza, M. Peterlechner, J. Freudenberger, G. Wilde, Acta Mater. 61 (1) (2013) 228–238.
[34] S.H. Xia, L.V. Vychigzhanina, J.T. Wang, I.V. Alexandrov, A.V. Sharafutdinov, Mater. Sci. Eng. A 490 (1–2) (2008) 471–476.
[35] X. Wu, M. Yang, F. Yuan, G. Wu, Y. Wei, X. Huang, Y. Zhu, Proc. Natl. Acad. Sci. 112 (47) (2015) 14501–14505.
[36] D.K. Yang, P.D. Hodgson, C.E. Wen, Scr. Mater. 63 (9) (2010) 941–944.
[37] J. Shen, B. Chen, X. Ye, H. Imai, J. Umeda, K. Kondoh, Mater. Des. 116 (2017) 99–108.
[38] D. Guo, M. Li, Y. Shi, Z. Zhang, H. Zhang, X. Liu, B. Wei, X. Zhang, Mater. Des. 34 (2012) 275–278.
[39] Y. Shi, M. Li, D. Guo, T. Ma, Z. Zhang, G. Zhang, X. Zhang, Mater. Lett. 108 (2013) 228–230.
[40] T.R. Lee, C.P. Chang, P.W. Kao, Mater. Sci. Eng. A 408 (1–2) (2005) 131–135.
[41] Z. Zhang, G. Zhang, D. Guo, M. Li, Y. Shi, X. Li, X. Zhang, Mater. Lett. 131 (2014) 240–243.
[42] L. Pantělejev, R. Štěpánek, O. Man, Mater. Charact. 107 (2015) 167–173.
[43] A. Rollett, F. Humphreys, G.S. Rohrer, M. Hatherly, Recrystallization and Related Annealing Phenomena, Elsevier2004.
[44] H.A. Murdoch, C.A. Schuh, J. Mater. Res. 28 (16) (2013) 2154–2163.
[45] J.A. Thornton, Annu. Rev. Mater. Sci. 7 (1) (1977) 239–260.
[46] W. Petry, Phase Transit. 31 (1–4) (1991) 119–136.
[47] E.S. Fisher, C.J. Renken, Phys. Rev. 135 (2A) (1964) A482–A494.
[48] G.F. Vander Voort, Metallography, principles and practice, ASM International1999.
[49] E. Bauer, J.H. van der Merwe, Phys. Rev. B 33 (6) (1986) 3657–3671.
[50] Q. Zhou, J.Y. Xie, F. Wang, P. Huang, K.W. Xu, T.J. Lu, Acta Mech. Sinica 31 (3) (2015) 319–337.
[51] J.M. Howe, Interfaces in materials: atomic structure, thermodynamics and kinetics of solid-vapor, solid-liquid and solid-solid interfaces, Wiley-Interscience1997.
[52] F. Cardarelli, Materials handbook: a concise desktop reference, Springer Science & Business Media2008.
[53] L. Vitos, A.V. Ruban, H.L. Skriver, J. Kollár, Surf. Sci. 411 (1–2) (1998) 186–202.
[54] M. Ohring, Mater. Sci. of thin films, Academic press2001.
[55] Y. Leng, Mater. Charact.: introduction to microscopic and spectroscopic methods, John Wiley & Sons2009.
[56] Á.K. Kiss, E.F. Rauch, B. Pécz, J. Szívós, J.L. Lábár, Microsc. Microanal. 21 (02) (2015) 422–435.
[57] J.A. Floro, S.J. Hearne, J.A. Hunter, P. Kotula, E. Chason, S.C. Seel, C.V. Thompson, J. Appl. Phys. 89 (9) (2001) 4886–4897.
[58] K.-N. Tu, J.W. Mayer, L.C. Feldman, Electronic Thin Film Science: For Electrical Engineering and Materials Scientist, Macmillan New York1992.
[59] M. Bobeth, A. Ullrich, W. Pompe, Destratification mechanisms in coherent multilayers, J. Metastable Nanocryst. Mater., Trans Tech Publ, 2004, p. 153.
[60] H. Mehrer, Diffusion in Solids: Fundamentals, Methods, Materials, Diffusion-Controlled Processes, Springer Berlin Heidelberg2007.
[61] R.D. Doherty, D.A. Hughes, F.J. Humphreys, J.J. Jonas, D.J. Jensen, M.E. Kassner, W.E. King, T.R. McNelley, H.J. McQueen, A.D. Rollett, Mater. Sci. Eng. A 238 (2) (1997) 219–274.
[62] C.M. Cepeda-Jiménez, J.I. Beltrán, A. Hernando, M.A. García, F. Ynduráin, A. Zhilyaev, M.T. Pérez-Prado, Acta Mater. 123 (2017) 206–213.
[63] L.E. Murr, Mass, 1975.
[64] H.B. Wan, Y. Shen, X. He, J. Wang, Jom 65 (3) (2013) 443–449.
[65] A. Misra, R.G. Hoagland, H. Kung, Philos. Mag. 84 (10) (2004) 1021–1028.
[66] K.A. Darling, A.J. Roberts, Y. Mishin, S.N. Mathaudhu, L.J. Kecskes, J. Alloys Compd. 573 (2013) 142–150.
[67] M. Kapoor, T. Kaub, K.A. Darling, B.L. Boyce, G.B. Thompson, Acta Mater. 126 (2017) 564–575.
[68] P.R. Cantwell, M. Tang, S.J. Dillon, J. Luo, G.S. Rohrer, M.P. Harmer, Acta Mater. 62 (2014) 1–48.
[69] S.J. Dillon, M. Tang, W.C. Carter, M.P. Harmer, Acta Mater. 55 (18) (2007) 6208–6218.
[70] C.S. Smith, Metallogr. Microstruct. Anal. 4 (6) (2015) 543–567.